Morphology and properties of neutralized chitosan-cellulose nanocrystals biocomposite films

F.A. Corsello[a], P.A. Bolla[b,e], P.S. Anbinder[c], M.A. Serradell[d,e], J.I. Amalvy[a], P.J. Peruzzo[a,e,*]

[a] Instituto de Investigaciones Fisicoquímicas Teóricas y Aplicadas, INIFTA (UNLP—CONICET CCT La Plata), Diag. 113 y 64 (B1904DPI), CC 16 Suc. 4, La Plata, Argentina
[b] Centro de Investigación y Desarrollo en Ciencias Aplicadas "Dr. Jorge J. Ronco", CINDECA (UNLP—CONICET CCT La Plata), Calle 47 N° 257 (B1900AJK), La Plata, Argentina
[c] Instituto de Física de Materiales Tandil—IFIMAT (UNCPBA), CIFICEN (UNCPBA-CICPBA-CONICET), Pinto 399, 7000 Tandil, Argentina
[d] Cátedra de Microbiología, Departamento de Ciencias Biológicas, Facultad de Ciencias Exactas, Universidad Nacional de La Plata (UNLP), 47 y 115 s/n, 1900 La Plata, Argentina
[e] Universidad Nacional Arturo Jauretche—UNAJ, Av. Calchaquí 6200, 1888 Florencio Varela, Argentina

ARTICLE INFO

ABSTRACT

Chitosan/cellulose nanocrystals (CH-CN) films were obtained by casting of dispersions, and treated with NaOH for neutralization proposes. The composition of films was varied from 1 to 10 wt.% of CN. Changes in the morphology of the systems were correlated with the different properties studied. FTIR revealed the presence of a weak interaction between the polymer matrix and nanofiller, confirmed by a slightly increase in thermal stability. SEM images suggested that incorporating CN amounts higher than 3 wt.% generates phase-segregated systems, and SAXS showed that CH avoid the typical organization of CN at concentrations below 5 wt.%. Improved performance against water was obtained in composite materials comparing to the pure polymer matrix, as well as CH and CH-CN films did not show antibacterial activity demonstrating that remnant acetic acid, when no neutralization step is done, plays an important role in this property.

© 2016 Elsevier Ltd. All rights reserved.

1. Introduction

The field of polymeric materials has grown considerably in the last thirty years due to a significant increase in consumption. However, this sector is one that has been affected by the global oil crisis, due to begin to dwindle hydrocarbons derived from this industry and with them the raw materials of traditional polymers are obtained. According to Association for the Study of Peak & Oil, 2050 oil production will be reduced by 50% [ASPO]. Therefore, there have been proposals regarding the future of raw materials and their sources to continue with the polymers production, and has led to growing interest in polymers derived from renewable sources. With this in mind, natural compounds have been proposed as feedstock for the preparation of polymeric materials, such as carbohydrates like starch or cellulose, or the use of natural oils (Desroches, Escouvois, Auvergne, Caillol, & Boutevin, 2012; Imre

& Pukánszky, 2015). The production of polymers from alternative renewable resources contributes to solving some of the concerns caused by the depletion of conventional petrochemical resources and adds to the areas seeking reduce environmental impact and are using green production procedures. However, the current high costs have limited the applications, which lead to continue the research in this area.

Chitosan (CH) is a biopolymer with high potential, used in a wide range of applications since it possesses unique biological properties, including biocompatibility, biodegradability, antibacterial activity, among others, allowing the development of systems in a variety of forms including powders, films and microparticles. Unlike synthetic polymers, this polymer presents no limitations on biocompatibility, biodegradability and toxicity as well as being naturally abundant and renewable (Kurita, Kaji, Mori, & Nishiyama, 2000; Ravi Kumar, 2006; Rinaudo, 2006). Although products based on CH have found a large number of industrial applications in different areas they have, as other biopolymers, lower mechanical and water resistance properties than traditional products. Therefore, different studies of this polymer has been continuous to respond to the demand for new and improved properties that are continually required. Some of those studies led to the incorporation of other materials (organic or inorganic) to a CH matrix, in an

---

* Corresponding author at: Instituto de Investigaciones Fisicoquímicas Teóricas y Aplicadas - INIFTA (UNLP – CONICET CCT La Plata), Diag. 113 y 64 (B1904DPI) La Plata, Argentina. CC 16 Suc. 4.
E-mail addresses: pjperuzzo@inifta.unlp.edu.ar, pjperuzzo@gmail.com (P.J. Peruzzo).

attempt to combine the characteristics of the original materials, to explore possible synergies between them and/or access to new properties. Such materials are intended mainly to biomedical and different short-term applications, such as packaging, agriculture and hygiene devices and sensors applications (Hein, Wang, Stevens, & Kjems, 2008; Jaiswal, Chauhan, & Sankararamakrishnan, in press; Sorrentino, Gorrasi, & Vittoria, 2007; Tanase & Spiridon, 2014). Therefore they represent a strong and emerging answer to obtaining high-performance and ecofriendly materials, representing an interesting alternative to traditional polymeric nanocomposites.

Cellulose Nanocrystals (CN) have gained particular attention in recent years as nanofiller material, not only for its unique physical and chemical properties, but also for its inherent capacity for renewal and sustainability, in addition to its abundance (Habibi, Lucia, & Rojas, 2010). As other biopolymers, even when CH present interesting mechanical properties, it has been studied the incorporation of CN nanofiller in order to improve the thermal and barrier properties of the obtained films based on the high aspect ratio of this nanofiller. The preparation and properties of CH based films reinforced with CN varying the nanofiller content has been reported by different authors, and commonly accompanied by the use of glycerol (G) as plasticizer (Azeredo et al., 2010; Dehnad, Emam-Djomeh, Mirzaei, Jafari, & Dadashi, 2014; Khan et al., 2012; Pereda, Dufresne, Aranguren, & Marcovich, 2014). In general, they found improved tensile strength, thermal and barrier properties (as water permeability) in films containing CN compared to pure CH. Most of the properties were favored by high concentrations of CN and low G content. Their results also demonstrated how the properties of the composite films can be controlled by adjusting the amount of incorporated CN and/or G; however, a detailed morphology-properties relationship is not always achieved. Other important factors are the acid used for the preparation of the CH solutions, and the application of a neutralization step during the de-casting of the films. Recently, Youssef, Abou-Yousef, El-Sayed, and Kamel (2015) have demonstrated the effects of the neutralization treatment on properties of CH-based nanocomposite films, in particular on mechanical properties. In general, this effect is not taken into account in most of the works where the properties of the CH-CN films could be affected (mechanical and water resistant behavior) (Azeredo et al., 2010; Dehnad et al., 2014; Khan et al., 2012; Pereda et al., 2014). Moreover, obtaining films containing CN well dispersed it is not easy to achieve. The large aspect ratio of the nanoparticle makes difficult an adequate dispersion and incorporation to the polymer matrix. In addition, the properties of these materials depend heavily on the polymer matrix characteristics and the nanofiller nature, and plasticizer and remnant organic acid could affect the morphology and properties of composites, for instance antimicrobial activity. This may partly explain the differences found in the literature for the variation of the properties and optimum compositions reported from the CH-CN bionanocomposites films, where all those factors are combined. Thus, in this work, chitosan/cellulose nanocrystals (CH-CN) nanocomposite neutralized films were obtained and the effect of varying the nanofiller content on the morphology and properties of these biocomposite materials was evaluated.

2. Material and methods

2.1. Materials

In this paper, Parafarm brand CH was used. The commercial CN was provided by the University of Mayne, which are rod-shaped particles of about 5 nm in diameter and 150 to 200 nm in length, obtained from cellulose pulp (information provided by the manu-

facturer). Sodium hydroxide and acetic acid used were analytical grade reagents mark ANEDRA.

2.2. Preparation of films

The required amount of CN was dispersed in 10 ml of acetic acid 1 v% for 30 min by magnetic stirring and subsequently sonicated for 30 min using a tip sonicator (Bandelin Sonopuls HD 60; tip Titanium TT 12; frequency 20 kHz; output power 37 W). The obtained dispersion was added drop by drop on 25 ml of a 2 wt% CH solution in acetic acid 1 v% with constant magnetic stirring, and subsequently sonicated for 15 min in above conditions. The resulting dispersions were submitted to vacuum to remove bubbles, and were deposited onto glass petri dishes (ϕ = 10 cm), then maintained 48 h at ambient T and further placed in an oven at 60 °C for 24 h. Films were treated with NaOH 10 wt% for neutralization and then with distilled water to neutral pH of the washing water. The films were allowed to dry at room temperature on Teflon® surfaces and reserved in desiccator (CaCl$_2$) previous to characterization. Samples containing 1, 3, 5 and 10 wt% of CN were prepared. Chitosan film was prepared as a reference material. Films with a thickness around 50 μm were obtained by the procedure described in this work. A shorthand notation is used in this paper to describe the composite systems: "CN3" denote a hybrid system prepared using 3 wt% of CN.

2.3. Characterization

The UV–visible spectra of films (0.250 mm thickness) were measured using a Genesys10S (Thermo Scientific) spectrometer in a wavelength range from 200 to 800 nm.

FTIR spectra of samples were obtained using a FTIR Nicolet 380 spectrophotometer in ATR mode (64 scans for experiment and a resolution of 4 cm^{-1}).

The morphology of the cross-section of the films was observed by Scanning Electron Microscopy (SEM) using a Jeol JSM-6460 microscope. The samples were immersed in liquid nitrogen to fracture and then were sputtered with a Au-Pd mixture before observation.

Small-angle X-ray scattering (SAXS) experiments were performed at the SAXS2 beamline at the National Laboratory of Synchrotron Radiation in Campinas, Brazil. A monochromatic beam with a wavelength of 1.608 Å and an exposure time of 60 s was used. Scattering intensity was registered using a two-dimensional detector with a sample detector distance of 2314.8 mm. One dimensional curves were obtained by integrating the two-dimensional data with the program FIT2D. The acquired data were corrected by subtracting the background contribution of the empty cell.

Thermal gravimetric analysis (TGA) were obtained using a Shimadzu DTG-60 instrument, running about 5 mg sample from room temperature to 600 °C at a heating rate of 10 °C min^{-1} in N$_2$ atmosphere.

Contact angle measurements have been carried out using a Model 500 goniometer (Ramé-Hart Instrument Co., USA) in the contact angle mode. Images were analyzed using the DROPimage Advanced v2.2 software. All the tests were performed on the air-facing surfaces of the samples. Six measurements on different points were performed to calculate the mean static contact angle, θ.

For the Water Uptake (WS) measurements, specimens 20 mm in diameter and 0.200 mm in thickness were prepared. They were immersed in distilled water at 25 °C. Specimens were periodically removed from water, and blotting with a filter paper to remove the surface adsorbed water followed by immediately weighing the films with a precision of 0.01 mg before being returned to the water bath. The relative mass uptake was determined as

$WS_t\% = [(W_t - W_0)/W_0].100$ were W_t and W_0 are the instantaneous and initial weights, respectively.

Tensile properties (such as tensile strength, elongation at break and stress at break) of the films were measured at 25 °C using a DIGIMESS TC-500 tensile-testing machine. Specimens of 0.050 mm thickness, 10.00 mm width and 50.00 mm length were prepared, and a testing speed of 5 mm min^{-1} was used. Results were the average of five valid measurements.

The Water Vapor Permeability (WVP) test was conducted gravimetrically. At first, the measurement cells filled with anhydrous calcium chloride desiccant to create a 0% RH storage condition and the surfaces of cells were covered with the films and sealed with molten paraffin. To maintain a 75% RH gradient across the film at 25 °C, a sodium chloride-saturated solution was used in the desiccator. The RH difference between two sides of the films creates a vapor pressure equal to 1753.55 Pa. Once steady state was reached, the cells were weighted at 1 day intervals during 5 days by a digital balance (GK1203, Sartorius Co., Germany) nearest to the 0.001 g. The slope of the weight loss versus time was obtained by linear regression. Water vapor permeability were calculated by the following equation: WVP = (Curve slope × Thickness)/(Area × Pressure difference).

To evaluate the antimicrobial activity, the effect of the films on pathogenic bacteria growth was tested. The pathogens used, *Shigella flexneri* ATCC 9199 and *Escherichia coli* Edl 933, were obtained from the Cátedra de Microbiología, Facultad de Ciencias Exactas, Universidad Nacional de La Plata. The working cultures were propagated into 50 ml sterilized nutrient broth (NB) (Biokard, Diagnostic, Beauvais, France) and were incubated overnight at 37 °C. The cell density was adjusted to 10^5 CFU/ml with fresh NB. An aliquot of 0.5 ml of cell suspension, 4.5 ml sterile NB and 2.5 mg film were mixed and incubated, in agitation, at 37 °C for 240 min. Serial dilutions of samples were prepared in 0.1% tryptone and plated on nutritive agar. The plates were incubated at 37 °C for 24 h in aerobic environment and the colonies were counted. Positive and negative controls of pathogen growth were included. Differences in survival rates of microorganisms were statistically tested by using Student *t*-test to determine any significant difference.

3. Results and discussion

The chitosan used in this work presented a viscosimetric molecular weight (Mv) of 310 kDa and a deacetylation degree (DD) of 95.2% obtained from FTIR spectra (Beil, Schamberger, Naumann, Machill, & van Pée, 2012). In the case of CN, it presented an average length and diameter 164 ± 31 nm and 7 ± 2 nm, respectively, obtained from TEM images (see the Supplementary information). The aspect ratio of the nanofiller based on these parameters was about 23, in agreement with typical values reported in other studies for similar materials (Habibi et al., 2010).

3.1. FTIR results

Fig. 1a shows the FTIR spectra of films of CH, CN and hybrid systems with different CN content. The signals observed in the CH and CN spectrums are similar to those described by different authors and are presented in detail in the Supplementary information file. In short, the main absorption peaks of pure CH are observed at 1647 cm^{-1} attributed to C=O stretching ($\upsilon_{C=O}$; Amide I band), at 1585 cm^{-1} assigned to a combination of N—H bending and C—N stretching vibrations ($\upsilon_{C-N} + \delta_{N-H}$; Amide II band), and the broad band above 3000 cm^{-1} is mainly assignable to the O—H stretching vibrations (υ_{OH}; 3500–3250 cm^{-1}) overlapped with the NH$_2$ stretching (υ_{NH}; 3400–3200 cm^{-1}). In addition, the medium to strong IR absorption bands at 1200–970 cm^{-1} are mainly due

to C—C and C—O stretching in pyranoid ring (Gómez-Ordóñez and Rupérez, 2011; Kačuráková, Capek, Sasinková, Wellner, & Ebringerová, 2000; Lagaron, Fernandez-Saiz, & Ocio, 2007). For the pure CN the band between 3600 and 3200 cm^{-1} was related to the O—H stretching vibrations, with a sharp peak located at 3337 cm^{-1} due to hydrogen bonded O—H stretching vibrations, and the absorption bands between 3000 and 2800 cm^{-1} and 1500–1250 cm^{-1} came from the C—H and C—H$_2$ stretching and bending vibrations. In addition, was also possible to observe the band related to the glycosidic linkage (1155 cm^{-1}) and the strongest band located between 1100–970 cm^{-1} dominated by ring vibrations overlapped with stretching vibrations of C—OH side groups, and at 1029 cm^{-1} the C—O—C stretching in the pyranoid ring (Gómez-Ordóñez & Rupérez, 2011; Kumar, Negi, Choudhary, & Bhardwaj, 2014). Due to the similar nature of the materials that conform the prepared nanocomposites, their spectra presented similar FTIR bands to the raw materials. However, a slight contribution of CN spectra was identified in the composite films, in particular by an increasing of the intensity of the OH stretching band in the region of hydrogen bonded O—H stretching, which is presented in detail in Fig. 1b. In addition, a small shift to lower wavenumbers was observed for the band located at 1066 cm^{-1}, related to stretching of C—O group in CH (see Fig. 1c), suggesting an interaction by hydrogen bonding between CH and CN.

3.2. SEM results

The morphology of the prepared films was observed by SEM and images are presented in Fig. 2. By observing the fracture surface, while the material containing 1 wt% of CN presented a roughness similar to the CH sample, the film containing 3 wt.% of nanofiller had a slightly rougher surface than that observed for pure CH. This effect was increased by incorporating an additional amount of CN, as can be seen in the fracture surface obtained for CN5 and CN10. This suggests a more homogeneous material distribution within the film for lower nanofiller load values. Observing the air-exposed surface of the film, although CH had and intrinsic surface roughness, the incorporation of CN to the polymeric matrix lead to the observation of aggregates, which would indicate that the incorporation of the reinforcing material is not completely homogeneous (for images see Supplementary information file).

3.3. SAXS results

SAXS analyses of films were done and Fig. 3 shows the SAXS profiles of the CH and the CH—CN nanocomposites obtained in this work. The scattering intensity depends on the distribution, electron density, size and the shape of the structure that causes X-ray scattering (de Oliveira Patricio et al., 2013). In our case, SAXS curves of composites showed features related to the contribution of CH matrix and CN particles, but changes were observed depending on the CN concentration. For CN dispersion, the corresponding Guinier plots ($\ln(I(q))$ *vs.* q^2) are convex and do not show any linear region satisfying $qRg \ll 1$ in the studied q range, which would be the case if the particles were described as monodisperse cylinders (Elazzouzi-Hafraoui et al., 2008). On the same way, pure chitosan and nanocomposites films did not present linearity on Guinier zone (for plots see Fig. S3 in the Supplementary information file). For all nanocomposite SAXS curves, we can observe broad scattering peaks with maximums in different q values. Characteristic distance (L) could be estimated from the q_{max} corresponding to the peak on $I(q)q^2$ *vs.* q curves and is defined as $L = 2\pi/q_{max}$. Nanocomposites L values were obtained from data plotted in Fig. 4 and could be seen in the figure inset. It is appreciable the increment in L values with the nanocrystal concentration. Pure CN presented a L value of 25.7 nm, which could be attributed to the CN aggregates
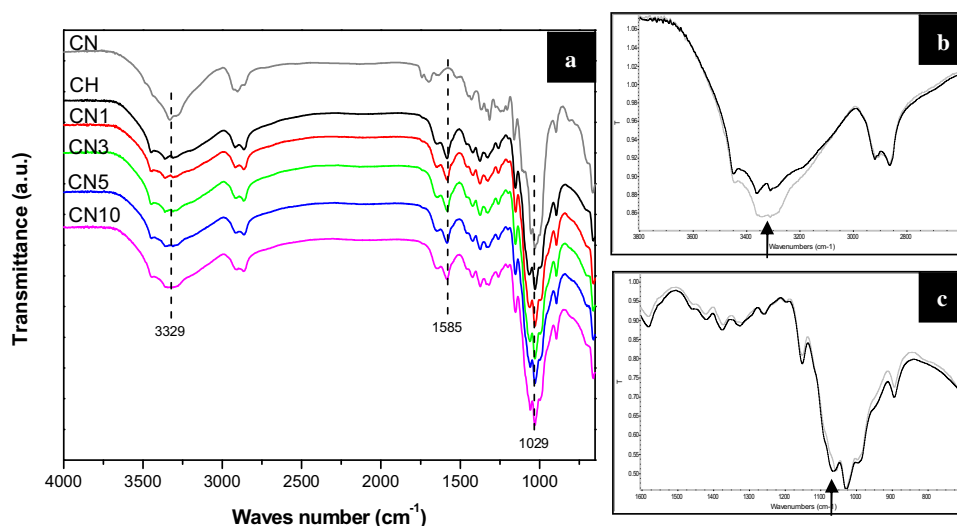
Fig. 1. (a) FTIR spectra of CH, CN and CH-CN samples prepared in this work. FTIR spectrum of CH (black) and CN10 (gray) in the 3800–2600 cm^{-1} region and 1600–700 cm^{-1} region are shown in b and c, respectively. Arrows indicate the main changes in the spectra.
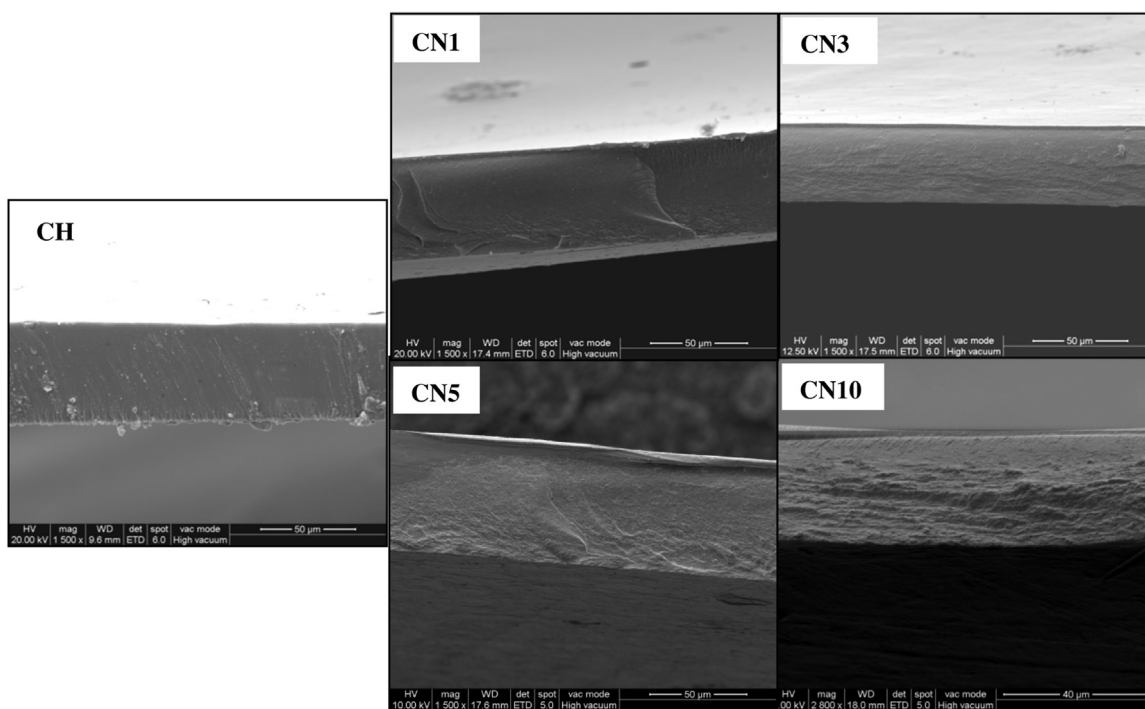
Fig. 2. SEM images of the fracture surface of samples prepared in this work.

width (Elazzouzi-Hafraoui et al., 2008; Uhlig et al., 2016). As seen below, while samples with CN contents up to 5 wt.% presented L distances around 16 nm, CN10 sample showed a L value similar to that obtained for CN dispersion. Elazzouzi et al. have also reported differences in aggregate sizes with the concentration of CN dispersions (Elazzouzi-Hafraoui et al., 2008). Non-homogeneous distribution of CN or too much long inter-domain lengths (not seen in the used q-range) could not allow us determines those inter-domain distances. Uhlig et al. (2016) have recently found values of 90–130 nm between CN aggregates in semi-diluted systems, and they suggest that the electrostatic interaction between the CN aggregates is not primarily controlling this structuring, and instead they use steric arguments to explain the observed differences in inter-aggregate distances. As consequence, we might say that, at low CN concentrations (below 5 wt%), CH could avoid the aggregation of CN, limiting

the typical organization for this nanoparticles in dispersion and this determined the film structure. Moreover, the proved interaction between CH and CN by hydrogen bonds, would also affect the properties of this nanocomposites.

3.4. Comparison of film properties

The high transmittance of films (T > 65%) obtained from UV–vis spectra in the 400–800 nm regions is in accordance with the high transparency observed in all these systems (see the Supplementary information).

TGA curves for selected films were represented in Fig. 4. A complete discussion of the behavior of CH and CN samples is presented in the Supplementary information file. In the CH film, the greatest weight loss identified at 296.4 °C obtained from DTGA curves.
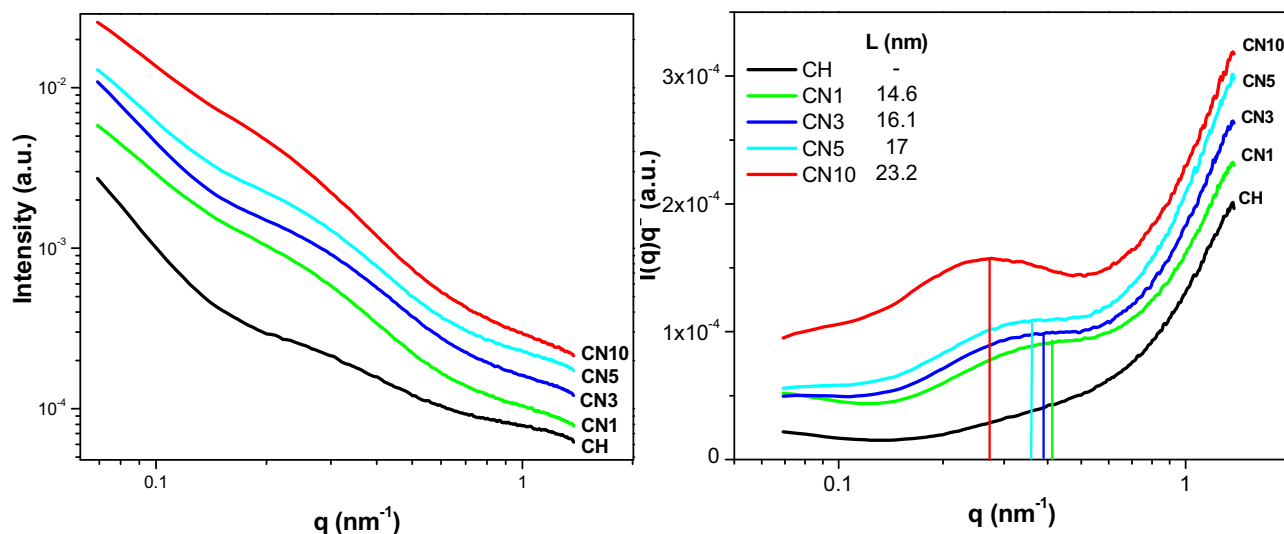
Fig. 3. SAXS curves I vs q (left) and Iq2 vs q plots (right) of CH and CH-CN films. Inset shows characteristic distance (L).

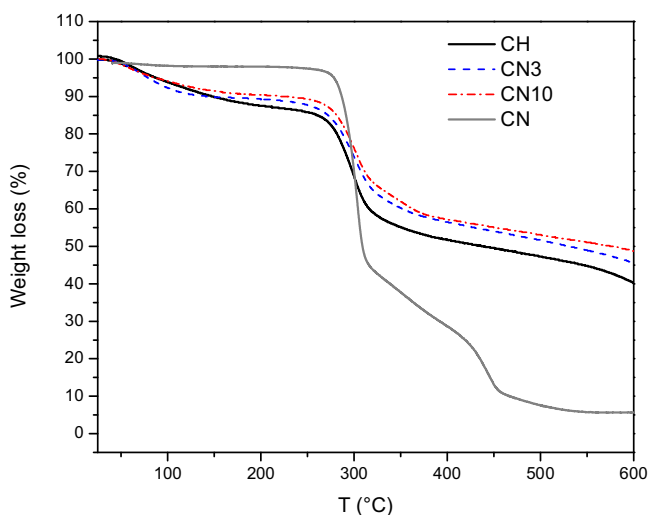**Fig. 4.** TGA curves of CH and CN, and CN3 and CN10 nanocomposite films.

Table 1
Mechanical properties, water sorption at 24 h (WS$_{24h}$), water contact angle (CA) and water permeability (WP) of films prepared in this work.

Sample	Mechanical properties			WS$_{24h}$ (%)	CA (°)	WP[a] (10^2)
	ε (%)	σ (MPa)	E (MPa)			
CH	10.8 ± 2.4	58.0 ± 8.3	13.5 ± 1.7	67.0 ± 1.2	82.7 ± 6.8	5.6
CN1	7.2 ± 1.1	59.1 ± 5.7	15.2 ± 3.9	70.8 ± 3.6	96.4 ± 2.2	3.7
CN3	9.3 ± 2.7	56.1 ± 2.9	19.9 ± 3.3	71.9 ± 3.3	95.6 ± 4.8	4.7
CN5	13.4 ± 4.5	68.2 ± 3.4	17.8 ± 5.1	65.4 ± 3.8	94.9 ± 3.4	3.5
CN10	13.8 ± 1.9	62.7 ± 2.6	13.8 ± 4.2	61.5 ± 3.6	92.5 ± 3.0	4.2

[a] Unit: [(g/d) cm]/[m² mmHg].

All samples containing CN showed similar thermal behavior to CH (Celebi and Kurt, 2015). The effect of incorporation of CN to the polymeric matrix was an increase in the maximum decomposition temperature of about 7 °C, based on the peaks observed in DTGA curves of CN10 and CN3 (303.3 °C), indicating a small increase in thermal stability respect to CH regarding the CN content. In addition, at higher CN contents was also possible to observe a clear contribution of the nanofiller thermal degradation profile, by the appearance of a small thermal degradation stage at about 350 °C, associated with the second decomposition step of the CN curves.

Mechanical properties of the films (Table 1) showed no changes in stress at break values (σ) with the addition of CN. However, observing the elongation at break and Young's modulus values (ε and E, respectively), slight changes were observed related to CN content. For ε, a decrease of this parameter with the addition of 1 wt% of CN was observed comparing to the pure matrix, with a further increase to reach a stable value for CN contents higher than 5 wt.%. Moreover, an increase of E as CN content increase was observed up to samples containing 3 wt.% of nanofiller, followed by a decreasing trend with a large scatter in the obtained values. Both ε decreasing and E increasing at low CN contents can be attributed to two factors: (1) nanocrystal-polymer interactions

and (2) stress transfer at the interface polymer-nanocrystal. At low concentrations, CN are homogeneously dispersed into the polymer matrix without interactions between them (Favier, Chanzy, & Cavaille, 1995), thus increasing the mechanical strength of the nanocomposite films may be due to an efficient load transfer to the nanocrystals network. Beyond 3 wt.% CN, the obtained results suggest that addition of CN above this threshold concentration helps not to improve the mechanical properties, which can be attributed to aggregation of particles CN after reaching a certain concentration (Khan et al., 2012), in agreement with SAXS results. However, from an applicative point of view, all the samples seems to have a similar mechanical behavior due to the slight changes observed as CN content increase, probably related to small contribution to the reinforcement of an strong matrix as chitosan by the incorporation of a nanofiller, and the slight interaction between CN and polymer matrix observed by FTIR.

The properties related to the behavior of the materials against water (water contact angle, water swelling degree, water vapor permeability) are presented in Table 1. All the samples presented water sorption curves with a fast initial water uptake behavior, followed by a smooth leveling of the sorption curve to a saturation level with a longer immersion time (for swelling curves see Supplementary information file). Observing the saturation levels obtained at 24 hs (WS$_{24h}$, Table 1), it can be noted that the CN has an effect on water uptake. For lower CN contents the trend is a slight increase of water uptake reaching maximum at 3 wt% of nanofiller content. An attempt to incorporate additional CN produced a decrease of this parameter. A possible explanation can be proposed based on the possibility to form paths through the film that favor the access of water for lower CN contents (Faucheu et al., 2010; Reyes, Peruzzo, Fernández, Paulis, & Leiza, 2013). On other hand, a decrease in

the water sorption of the nanocomposites related to the unfilled matrix for higher CN contents is probably due to a barrier effect associated with the large nanoparticles that physically blocked the penetration of water molecules.

In general, a slight increase of water contact angle of the films prepared in this work was observed as the CN content increase, compared to the pure CH sample. This tendency indicated the presence of a more hydrophobic surface, which is different to the trend observed by Celebi and Kurt for this system at high CN contents (Celebi & Kurt, 2015), probably due to increased roughness and the heterogeneity of the surfaces of these samples.

WVP values decreased with the addition of CN. The presence of CN is believed to increase tortuosity in the polymer matrix films, which leads to slower water vapor diffusion processes and thus reduced permeability (Azeredo et al., 2010).

For the purpose of assessing whether the nanocomposite films affect microbial growth, inhibitory effect against intestinal pathogens was studied (Fig. 5). A small inhibitory effects of CH films on *E. coli*, and no effect on *S. flexneri* were observed. As expected, the incorporation of CN did not modify the intrinsic inhibitory effect of chitosan and no correlation with CN content was observed in our experimental conditions.

Comparing to other works reported in the literature (Azeredo et al., 2010; Dehnad et al., 2014; Khan et al., 2012), in our case is notable the slight changes observed in the properties of CH-CN films as CN content increase, but are in agreement with the results presented recently by Celebi and Kurt (2015). When our samples were obtained without using a neutralization step, a first remark is that was not possible to handle them after being immersed in water or exposed to water during contact angle studies, and they became soft and broke after immersion at long times. This is clearly related to presence of acetic acid residue in the films, as could be observed by FTIR (see Fig. S9 in Supplementary information file), which in contact with water allows the protonation of amino groups of chitosan and produce the dissolution of the chitosan films at this condition. In addition, the films that were not neutralized showed a marked inhibition (7 log) of *E. coli* growth as shown in Fig. 5a, and induced a reduction of 2–3 logs on *S. flexneri* growth (Fig. 5). Lower pH increases the antimicrobial activity of chitosan, in addition to the 'hurdle effect' of inflicting acid stress on the target organisms (Dutta, Tripathi, Mehrotra, & Dutta, 2009). Thus, beyond the intrinsic inhibitory power of the polymer matrix of the nanocomposite films prepared in this study, the inhibitory power of non-neutralized films could be awarded to the content of acetic acid present in these samples. This is in agreement with previous results that revealed that chitosan as such is not an antimicrobial agent against *Staphylococcus aureus* and that only as chitosonium acetate films show optimum biocide properties due to the presence of protonated or "activated" amine groups at this condition (Fernandez-Saiz, Lagaron, & Ocio, 2009). Moreover, when these authors used a control solution of acetic acid that matches the pH of the chitosan solution sample does not showed a significant bacterial inhibitory effect. Thus, beyond the intrinsic inhibitory power of the polymer matrix of the nanocomposite films prepared in this study, the inhibitory power of non-neutralized films could be awarded to the content of acetic acid present in these samples and confirmed by FTIR (see Fig. S9 in Supplementary information file).

Surprisingly, in most works non-neutralized films were studied. In this way, changes in different properties could be related to effects due to the presence of remnant organic acid which could act as plasticizer, in addition to protonate the amine groups being charged the chitosan chain, which can affect interactions between polymer matrix and the nanofiller. Thus, in those works, is possible to find water swelling values up to 400% (Khan et al., 2012), water solubility values of the biocomposite films between 20 and 50% or

an increase of WVP as CN content increase (Dehnad et al., 2014), and even FTIR bands assignments and interpretation based on FTIR spectrums containing remnant acid (for instance, compare Fig. 4 reported in Khan et al. (2012) with Fig. S9 of the Supplementary information File). Youssef et al. (2015) observed that the behavior of chitosan films were remarkably affected by different preparation parameter such us the type of acid for chitosan solvation, and using of concentrated alkali to assist for film removal. They concluded that the de-casting process of the films was preferred without using NaOH solution since films removal by neutralization suffer severe shrinkage (not soluble in water), while films containing organic acids presented better mechanical properties (but water soluble). Different to this, and based on the reported information and our results, we think that the neutralization process is an important variable. In this way, the study of the optimization of the neutralization process is a central issue to obtain a balance between the properties, in addition to other variables (chitosan molecular weight and deacetylation degree, different cellulose nanocrystals).

4. Conclusions

Chitosan/cellulose nanocrystals (CH/CN) nanocomposite neutralized films obtained by casting were characterized to investigate the effect of varying the nanofiller content on the resulting morphology and film properties. Results demonstrated the presence of interactions between the nanofiller and the polymer matrix, and a good incorporation of the cellulose nanocrystals was obtained at concentrations below 5 wt% by the method used in this work in agreement with SEM and SAXS results, where, in the later, increasing cellulose nanocrystals content lead to systems with characteristics length found for CN. Bionanocomposite films showed slight improved performance compared to the polymer matrix (surface hydrophobicity increase, water permeability decrease, water swelling decrease). Antimicrobial activity did not show changes regarding CN content, but it was found an important inhibitory effect when non-neutralized samples were used due to remnant acetic acid in the films. CN reinforced CH bionanocomposite films should have a promising impact in different areas due to the improvement of the properties of these materials. However, neutralization process must be taken into account during the preparation of CH-based nanocomposites since it affects the properties of these materials, with a high impact on the water resistance (improved) and antibacterial properties (worsened), among other effects on organoleptic properties related to the presence of organic acid residues that could limiting their application. An optimization of the NaOH treatment in the design of CH-based nanocomposite active films is necessary in order to obtain a balance between the final properties of these materials.

Acknowledgments

Appendix A. Supplementary data

Supplementary data associated with this article can be found, in the online version, at http://dx.doi.org/10.1016/j.carbpol.2016.09.031.
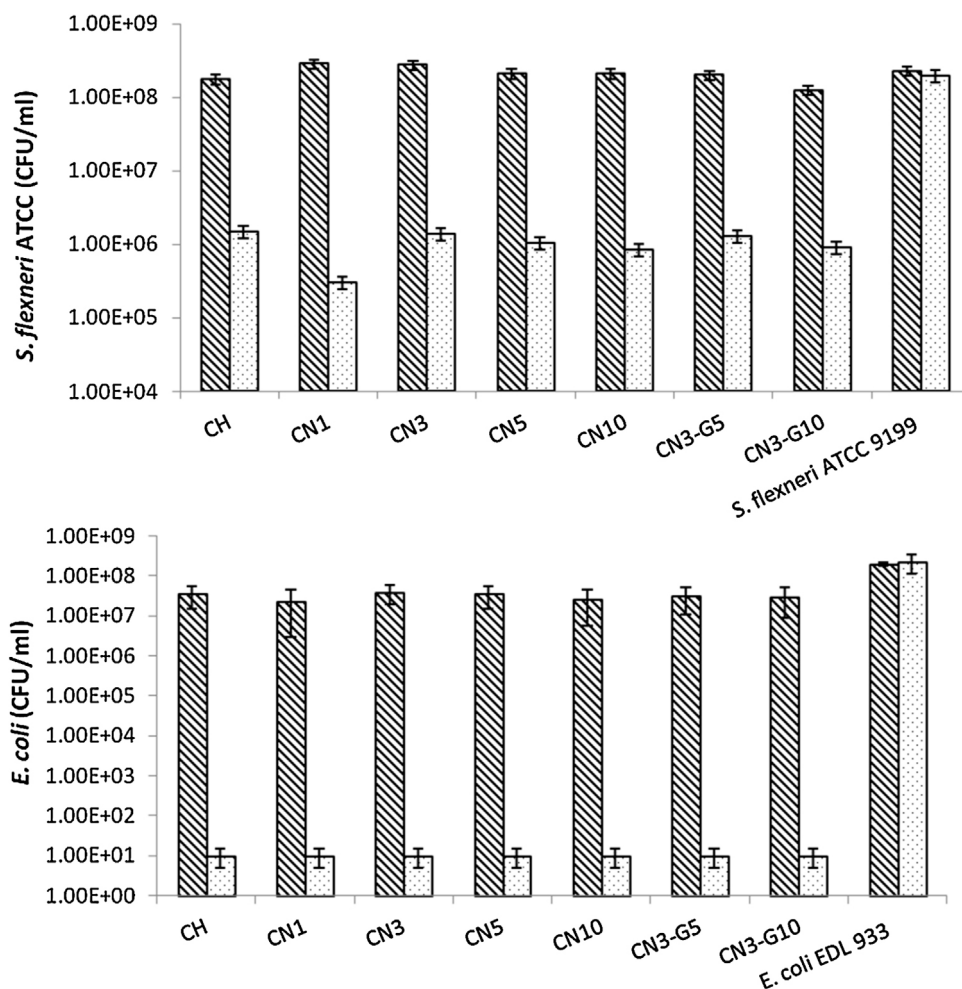
Fig. 5. Number of pathogen survival at different film composition. (Neutralized films/ Non- Neutralized films).

References

Association for the Study of Peak & Oil—www.peak-oil.org.

Azeredo, H. M., Mattoso, L. H., Avena-Bustillos, R. J. A., Filho, G. C., Munford, M. L., & Wood, D. (2010). Nanocellulose reinforced chitosan composite films as affected by nanofiller loading & plasticizer content. Journal of Food Science, 75, 19–28.

Beil, S., Schamberger, S., Naumann, W., Machill, S., & van Pée, K.-H. (2012). Determination of the degree of N-acetylation (DA) of chitin and chitosan in the presence of water by first derivative ATR FTIR spectroscopy. Carbohydrate Polymers, 87, 117–122.

Celebi, H., & Kurt, A. (2015). Effects of Processing on the properties of chitosan/cellulose nanocrystal films. Carbohydrate Polymers, 133, 284–293.

de Oliveira Patricio, P. S., Miranda Pereira, I., Ferreira da Silva, N. C., Ayres, E., Vargas Pereira, F., & Lambert Oréfice, R. (2013). Tailoring the morphology and properties of waterborne polyurethanes by the procedure of cellulose nanocrystal incorporation. European Polymer Journal, 49, 3761–3769.

Dehnad, D., Emam-Djomeh, Z., Mirzaei, H., Jafari, S.-H., & Dadashi, S. (2014). Optimization of physical and mechanical properties for chitosan—Nanocellulose biocomposites. Carbohydrate Polymers, 105, 222–228.

Desroches, M., Escouvois, M., Auvergne, R., Caillol, S., & Boutevin, B. (2012). From vegetable oils to polyurethanes: Synthetic routes to polyols and main industrial products. Polymer Reviews, 52, 38–79.

Dutta, P. K., Tripathi, S., Mehrotra, G. K., & Dutta, J. (2009). Perspectives for chitosan based antimicrobial films in food applications. Food Chemistry, 114, 1173–1182.

Elazzouzi-Hafraoui, S., Nishiyama, Y., Putaux, J.-L., Heux, L., Dubreuil, F., & Rochas, C. (2008). The shape and size distribution of crystalline nanoparticles prepared by acid hydrolysis of native cellulose. Biomacromolecules, 9, 57–65.

Faucheu, J., Gauthier, C., Chazeau, L., Cavaillé, J.-Y., Mellon, V., Pardal, F., et al. (2010). Properties of polymer/clay interphase in nanoparticles synthesized through in-situ polymerization processes. Polymer, 51, 4462–4471.

Favier, V., Chanzy, H., & Cavaille, J. Y. (1995). Polymer nanocomposites reinforced by cellulose whiskers. Macromolecules, 28, 6365–6367.

Fernandez-Saiz, P., Lagaron, J. M., & Ocio, M. J. (2009). Optimization of the biocide properties of chitosan for its application in the design of active films of interest in the food area. Food Hydrocolloids, 23, 913–921.

Gómez-Ordóñez, E., & Rupérez, P. (2011). FTIR-ATR spectroscopy as a tool for polysaccharide identification in edible brown and red seaweeds. Food Hydrocolloids, 25, 1514–1520.

Habibi, Y., Lucia, L. A., & Rojas, O. J. (2010). Cellulose nanocrystals: Chemistry, self-assembly and applications. Chemical Reviews, 110, 3479–3500.

Hein, S., Wang, K., Stevens, W. F., & Kjems, J. (2008). Chitosan composites for biomedical applications: Status, challenges and perspectives. Materials Science and Technology, 24, 1053–1061.

Imre, B., & Pukánszky, B. (2015). From natural resources to functional polymeric biomaterials. European Polymer Journal, 68, 481–487.

Jaiswal, M., Chauhan, D., & Sankararamakrishnan, N. (2016). Copper chitosan nanocomposite: Synthesis, characterization, and application in removal of organophosphorous pesticide from agricultural runoff. Environmental Science and Pollutant Research, 19, 2055–2062, in press

Kačuráková, M., Capek, P., Sasinková, V., Wellner, N., & Ebringerová, A. (2000). FT-IR study of plant cell wall model compounds: Pectic polysaccharides and hemicelluloses. Carbohydrate Polymers, 43, 195–203.

Khan, A., Khan, R. A., Salmieri, S., Le Tien, C., Riedl, B., Bouchard, J., et al. (2012). Mechanical and barrier properties of nanocrystalline cellulose reinforced chitosan based nanocomposite films. Carbohydrate Polymers, 90, 1601–1608.

Kumar, A., Negi, Y. S., Choudhary, V., & Bhardwaj, N. K. (2014). Characterization of cellulose nanocrystals produced by acid-hydrolysis from sugarcane bagasse as agro-waste. Journal of Materials Physics and Chemistry, 2, 1–8.

Kurita, K., Kaji, Y., Mori, T., & Nishiyama, Y. (2000). Enzymatic degradation of beta-chitin: Susceptibility and the influence of deacetylation. Carbohydrate Polymer, 42, 19–21.

Lagaron, J. M., Fernandez-Saiz, P., & Ocio, M. J. (2007). Using ATR-FTIR spectroscopy to design active antimicrobial food packaging structures based on high molecular weight chitosan polysaccharide. Journal of Agricultural and Food Chemistry, 55, 2554–2562.

Pereda, M., Dufresne, A., Aranguren, M. I., & Marcovich, N. E. (2014). Polyelectrolyte films based on chitosan/olive oil and reinforced with cellulose nanocrystals. Carbohydrate Polymers, 101, 1018–1026.

Ravi Kumar, M. N. V. (2006). A review of chitin and chitosan applications. Reactive & Functional Polymers, 46, 1–27.

Reyes, Y., Peruzzo, P. J., Fernández, M., Paulis, M., & Leiza, J. R. (2013). Encapsulation of clay within polymer particles in a high-solids content aqueous dispersion. *Langmuir, 29*, 9849–9856.

Rinaudo, M. (2006). Chitin and chitosan: Properties and applications. *Progress in Polymer Science, 31*, 603–632.Sorrentino, A., Gorrasi, G., & Vittoria, V. (2007). Potential perspectives of bio-nanocomposites for food packaging applications. *Trends in Food Sciences & Technology, 18*, 84–95.

Tanase, C. E., & Spiridon, I. (2014). PLA/chitosan/keratin composites for biomedical applications. *Materials Science and Engineering C, 40*, 242–247.

Uhlig, M., Fall, A., Wellert, S., Lehmann, M., Prévost, S., Wagberg, L., et al. (2016). Two-dimensional aggregation and semi-dilute ordering in cellulose nanocrystals. *Langmuir, 32*, 442–450.

Youssef, A. M., Abou-Yousef, H., El-Sayed, S. M., & Kamel, S. (2015). Mechanical and antibacterial properties of novel high performance chitosan/nanocomposite films. *International Journal of Biological Macromolecules, 76*, 25–32.